ROBUST FORCE AND IMPEDANCE CONTROL OF SERIES ELASTIC ACTUATORS

Luiza Mesquita Sampaio do Amaral, lu_amaral@uol.com.br
Bruno Jardim, bjfisica@gmail.com
Adriano Almeida Gonçalves Siqueira, siqueira@sc.usp.br
University of São Paulo at São Carlos, Mechanical Engineering Department, Mechatronics Laboratory, Av. Trabalhador São-carlense, 400 - São Carlos, SP, Brazil

Abstract. *This paper deals with robust $\mathscr{H}_\infty$ force and impedance control of series elastic actuators. It is considered that the series elastic actuators are subject to parametric uncertainties and external disturbances. Robust controllers based on the $\mathscr{H}_\infty$ criterion have been widely used among robotic applications for guaranteeing good disturbance rejection properties. The $\mathscr{H}_\infty$ force and impedance controls proposed in this paper will be implemented in an exoskeleton for lower limbs where the joints are actuated by a set of series elastic actuators. The results shows that the $\mathscr{H}_\infty$ force controller increased the bandwidth over the PID controller and rejects external disturbances properly. Also, the impedance controller works properly, with the the end-effector of the series elastic actuator following the desired trajectory generated by the controller regarding the desired impedance.*

Keywords: *Robust control, force control, series elastic actuator.*

1. INTRODUCTION

The interface between an actuator and its load is commonly designed to be as rigid as possible, Pratt and Williamson (1995). Increasing stiffness improves precision, stability and position control bandwidth. However, the use of such interface may incur friction, torque oscillations and noise. According to Pratt and Pratt (1998), an non-rigid interface is generally required when there is human-machine contact. In these cases, unexpected contacts and external disturbances may be avoided to not harm the user. Examples of devices where human-machine interaction is present are exoskeleton and active orthoses.

Exoskeletons are being developed around the world to help physically weak or injured people and to increase the power of soldiers. The BLEEX (Berkeley Lower Extremity Exoskeleton), project support by the Defense Advanced Research Projects Agency (DARPA), uses hydraulic actuators supplied by a pump connected into a small gasoline engine Kazerooni (2005); Zoss *et al.* (2005); Chu *et al.* (2005). More than 40 sensors together with the actuators form a local net that works as the human nervous system Kim *et al.* (2004). The sensors constantly give information to the central computer that calculates the necessary action to distribute the weight in such a way that the soldier does not feel the exceeding weight. In Walsh *et al.* (2006), an underactuated and lightweight exoskeleton that considers the passive dynamic of walking, differently of the one described above, is being developed. Two architectures are explored: the first one considers a spring in the hip, a variable impedance device in the knee and a spring in the ankle; the second one substitutes the spring of the hip by a no conservative actuator to examine the effect of power addition during the walking cycle. In Pratt *et al.* (2004), series elastic actuators (SEAs) are used in the development of a device for power augmentation of the knee joint. The same actuator is used in Blaya and Herr (2004) to drive an active ankle-foot orthosis specially designed to deal with the drop foot pathology.

Series elastic actuators are considered in this work since they present ideal characteristics for use in human-machine interaction: force control, impedance control (possibility of low impedance), impact absorption, low friction and bandwidth Robinson *et al.* (1999); Sensinger and Weir (2006). The idea behind the SEA is the inclusion of an elastic component between the motor's output and the load. The measurement of the elastic deformation is related to the applied load force by the dynamic characteristic of the spring.

In this paper, the first results of robust $\mathscr{H}_\infty$ force and impedance control of SEAs are presented. It is considered that the SEAs are subject to parametric uncertainties and external disturbances. Robust controllers based on the $\mathscr{H}_\infty$ criterion have been widely used among robotic applications for guaranteeing good disturbance rejection properties Chen *et al.* (1994); Chang (2000); Sage *et al.* (1999). The $\mathscr{H}_\infty$ norm defines the level of attenuation in the input/output relationship between the disturbance and the controlled output. The $\mathscr{H}_\infty$ force and impedance control proposed in this paper will be implemented in an exoskeleton for lower limbs where the joints are actuated by a set of SEAs.

This paper is organized as follows: Section 2. presents the proposed exoskeleton for lower limbs design, a short description of an SEA and its dynamic model; Section 3presents the $\mathscr{H}_\infty$ force control design; Section 3presents the $\mathscr{H}_\infty$ impedance control design; and Section 5. presents the results of the force and impedance control, with some analysis of its efficiency.

2. SERIES ELASTIC ACTUATORS

In this section, the design and construction of the exoskeleton for lower limbs based on a commercial orthosis being developed by the authors. The commercial orthosis corresponds to one reciprocating gait orthosis LSU (Lousiana State University). Figure 1 shows the orthosis and the first exoskeleton design.

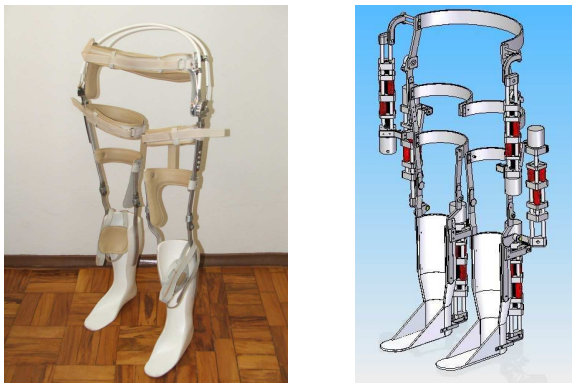

Figure 1. Commercial orthosis and exoskeleton design.

Traditional technologies for force control include current control with direct drive or geared actuator, force feedback through load cells, and fluid pressure control. In a direct drive actuator, a high quality servomotor is directly connected to the load and the torque output is accurately controlled using the relation between motor torque and motor current. However, servomotors operate inefficiently at the low speeds and high torques required in most robotic applications, which results in large and heavy units.

Alternatively, smaller and lighter servomotors can be used in low speed/high torque applications if a gear reduction is used. The reduction allows the motor to operate in high speed/low torque. However, the reduction gear has a few drawbacks such as friction and increasing the reflected inertia at the output of the gearbox. Since the factor of reduction is very large, the impedance increases and control of force becomes inaccurate.

Even in the case of a geared actuator, you can minimize the friction and the effects of inertia by controller, measuring the force by a load cell. However, a load cell induces instabilities. In the case of a very fast linear motion, it can generate a pulse of very high strength. To maintain system stability is necessary small controller's gains. Therefore, the control is too slow, not responding to low-amplitude desired forces.

To overcome these shortcomings, the authors of Pratt and Williamson (1995) proposed a force-controlled actuator, whose force sensor is a elastic element positioned in series with the load. This configuration is named Series Elastic Actuator.

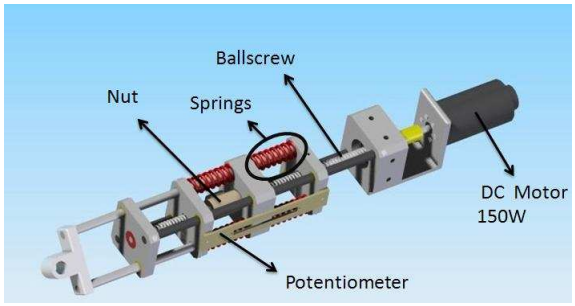

Figure 2. Series Elastic Actuator configuration.

The SEA presented in Robinson *et al.* (1999), reproduced in the Figure 2, consists of a DC motor fixed to a ball screw through elastic coupling. The platform motion is driven by the nut, which converts the rotational ball screw movement into linear movement of the platform. To obtain force and impedance control of the actuator it is introduced a set of springs between the platform and the end effector. When the DC motor is driven, the nut moves forward or backward, compressing the pair of springs. The springs apply force to the load through the end effector.

Force and impedance controls are done by measuring the spring deflection using a linear sliding potentiometer fixed in the two support platforms of the springs. Since the platforms are fixed in the two guides, the distance between them does not change. The potentiometer cursor is fixed in a nut support platform. When it moves, compressing the springs, the cursor moves up together, generating a voltage proportional to the springs deformation. By the Hooke's law, $F = -kx$, the force applied to the load is calculated.

The SEA shown in Figure 3, a similar reproduction of that presented in Robinson *et al.* (1999), was constructed and assembled in our laboratory. To control the SEA, a power driver *EPOS* 70/10 (Maxon Motor), and a software developed in *Borland Builder C + +* is used.

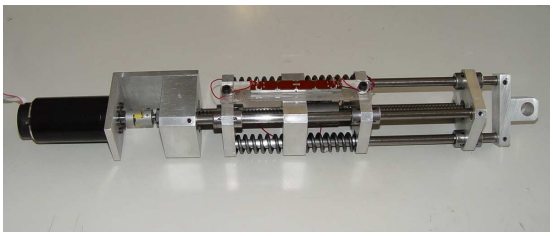

Figure 3. Series Elastic Actuator.

2.1 Dynamic Model and Force Control

The SEA is modeled as a simple mass-spring-damper system, with equivalent motor mass m_m, damper coefficient b_m, and elastic constant k, given by:

$$m_m\ddot{x}_m + b_m\dot{x}_m = F_m - F_l, \tag{1}$$

with

$$F_l = k(x_m - x_l), \tag{2}$$

where x_m is the linear position of the lead-screw nut, x_l is the load position, F_m is the force generated by the motor and output force F_l. Actually, the damper coefficient b_m is found from the force and velocity constraint of the DC motor Paluska and Herr (2006), that is,

$$b_m = \frac{F_{max}}{V_{max}}, \tag{3}$$

where F_{max} and V_{max} are maximum force and velocity the DC motor can reach, respectively. According to Walsh *et al.* (2006), this estimate is considered a first approximation for the limitations of the DC motor and it is very similar to the limitations observed for a biological muscle.

Therefore, the force driving the load, F_l, is function of F_m and x_l, and can be given in transfer function representation as:

$$F_l(s) = \frac{F_m(s) - (m_m s^2 + b_m s)x_l(s)}{\frac{m_m}{k}s^2 + \frac{b_m}{k}s + 1}. \tag{4}$$

In this paper it is assumed the load is fixed, that is, $x_l(s) = 0$. In this case, the force F_l is given by:

$$F_l(s) = \frac{F_m(s)}{\frac{m_m}{k}s^2 + \frac{b_m}{k}s + 1}. \tag{5}$$

We can also consider the existence of parametric uncertainties and the actuation external disturbances on the plant input. These perturbations are grouped in a combined disturbance $w(t)$. The state space representation of SEAs, regarding the above assumptions, can be computed as:

$$\begin{aligned} \dot{x}(t) &= A_p x(t) + B_{1_p} u(t) + B_{2_p} w(t) \\ y(t) &= C_p x(t) + D_p u(t) \end{aligned} \tag{6}$$

where $x(t) = [F_l\ \dot{F}_l]$ is the state, $y(t)$ is the measured output, $u(t)$ is the control input, and

$$A_p = \begin{bmatrix} 0 & I \\ -\frac{K_s}{m_m} & -\frac{b_m}{m_m} \end{bmatrix}, \quad B_{1_p} = B_{2_p} \begin{bmatrix} 0 \\ \frac{K_s}{m_m} \end{bmatrix},$$

$$C_p = \begin{bmatrix} 1 & 0 \end{bmatrix}, \quad D_p = \begin{bmatrix} 0 \end{bmatrix}.$$

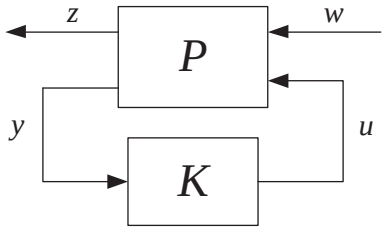

Figure 4. Block diagram for $\mathscr{H}_\infty$ control systems.

3. $\mathscr{H}_\infty$ FORCE CONTROL

In this section we present the basics of linear $\mathscr{H}_\infty$ control design and the procedures to apply it for robust force control of SEAs. We refer the reader to the vast literature on the subject for more details (see, e.g., Safonov *et al.* (1989) and Zhou *et al.* (1995)). The system is described by the block diagram in Figure 4, which shows the plant $P(s)$ and the controller $K(s)$. The plant has two sets of input signals, the internal input u and the external input *w*, and two sets of output signals, the measured signal *y* and the regulated output *z*.

As we are interested in the state-space form of the augmented system $P(s)$, we redefine the control system in the time domain as:

$$\begin{aligned} \dot{x}(t) &= Ax(t) + B_1 w(t) + B_2 u(t) \\ z(t) &= C_1 x(t) + D_{11} w(t) + D_{12} u(t) \\ y(t) &= C_2 x(t) + D_{21} w(t) + D_{22} u(t) \end{aligned} \tag{7}$$

where the state space matrices for the force control of SEA will be defined later.

The objective of an $\mathscr{H}_\infty$ controller is to guarantee that the $\mathscr{H}_\infty$ norm of a multivariable transfer function $T_{zw}(s)$ is limited by a level of attenuation γ, $\|T_{zw}(s)\|_\infty < \gamma$. The parameter γ indicates the level of robustness of the control system, or how much the input disturbances are attenuated in the output of the system. The following assumptions are required to design a simplified version of the $\mathscr{H}_\infty$ controller, based on the system (7):

(A1) (A, B_2) is stabilizable and (C_2, A) is detectable;

(A2) $D_{11} = 0$ and $D_{22} = 0$;

(A3) $D_{12}^T C_1 = 0$ and $B_1 D_{21}^T = 0$;

(A4) $D_{12} = \begin{bmatrix} 0 \\ I \end{bmatrix}$ and $D_{21} = \begin{bmatrix} 0 & I \end{bmatrix}$;

(A5) $\begin{bmatrix} A - j\omega I & B_2 \\ C_1 & D_{12} \end{bmatrix}$ has full column rank for all $\omega \in \mathbb{R}$;

(A6) $\begin{bmatrix} A - j\omega I & B_1 \\ C_2 & D_{21} \end{bmatrix}$ has full row rank for all $\omega \in \mathbb{R}$.

To synthesize the $\mathscr{H}_\infty$ controller we need to solve the following two algebraic Riccati equations associated with the state feedback control and the state estimate of the robot

$$\begin{aligned} &X_\infty (A - B_2 D_{12}^T C_1) + (A - B_2 D_{12}^T C_1)^T X_\infty + \\ &\quad X_\infty (\gamma^{-2} B_1 B_1^T - B_2 B_2^T) X_\infty + \hat{C}_1^T \hat{C}_1 = 0 \end{aligned} \tag{8}$$

and

$$\begin{aligned} &(A - B_1 D_{21}^T C_2) Y_\infty + Y_\infty (A - B_1 D_{21}^T C_2)^T + \\ &\quad Y_\infty (\gamma^{-2} C_1 C_1^T - C_2 C_2^T) Y_\infty + \hat{B}_1 \hat{B}_1^T = 0 \end{aligned} \tag{9}$$

where $\hat{C}_1 = (I - D_{12} D_{12}^T) C_1$ and $\hat{B}_1 = B_1 (I - D_{21}^T D_{21})$.

A stabilizing solution for this controller can be found if the matrices X_∞ and Y_∞ are positive semi-definite and the spectral radius of $X_\infty Y_\infty$ satisfies $\rho(X_\infty Y_\infty) \leq \gamma^2$. The design problem consists of finding minimum γ that obeys this inequality, thus yielding the "best" robustness. The family of all stabilizing controllers K_∞ that satisfy $||\mathscr{F}(P,K)||_\infty \leq \gamma$ is

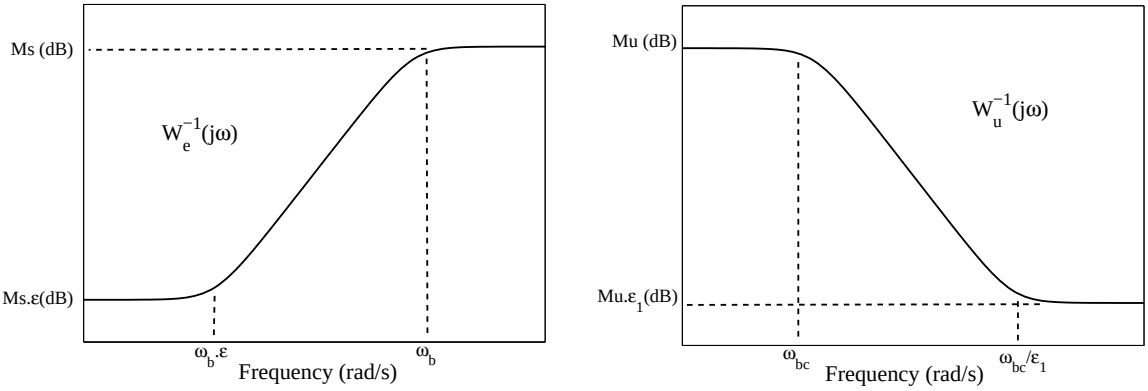

Figure 5. Weighting functions $W_e^{-1}(s)$ and $W_u^{-1}(s)$.

given by $K_\infty = \mathscr{F}(J,Q)$) where Q is any stable transfer function such that $||Q||_\infty < \gamma$, $\mathscr{F}(.,.)$ represents a linear fractional transformation, and

$$J = \begin{bmatrix} J_{11} & J_{12} \\ J_{21} & J_{22} \end{bmatrix} \tag{10}$$

where

$$\begin{aligned}
J_{11} &= A + B_2F_\infty + \gamma^{-2}B_1B_1^TX_\infty + Z_\infty H_\infty(C_2 + \gamma^{-2}D_{21}B_1^TX) \\
J_{12} &= \begin{bmatrix} -Z_\infty H_\infty & -Z_\infty(B_2 + \gamma^{-2}Y_\infty C_1^T D_{12} \end{bmatrix} \\
J_{21} &= \begin{bmatrix} F_\infty \\ -(C_2 + \gamma^{-2}D_{12}B_1^TX_\infty) \end{bmatrix}, \; J_{22} = \begin{bmatrix} 0 & I \\ I & 0 \end{bmatrix} \\
F_\infty &= -(B_2^TX_\infty + D_{12}^TC_1), \; H_\infty = -(Y_\infty C_2^T + B_1D_{21}^T), \\
Z_\infty &= (I - \gamma^{-2}Y_\infty X_\infty)^{-1}.
\end{aligned}$$

The design of the robust controller is performed considering the nominal model and weighting functions specially selected to improve controller performance. We start by finding a state-space realization of the augmented plant $P(s)$ through the definition of the performance objectives $W_e(s)$ and $W_u(s)$, which are related to the frequency response of the sensitivity function $S(s) = (I + P(s)K(s))^{-1}$, where $K(s)$ is the robust controller. To define $W_e(s)$, we select a bandwidth ω_b, a maximum peak M_s, and a small $\varepsilon > 0$. With these specifications in hand, the following performance-shaping, diagonal weighting matrix can be determined:

$$W_e(s) = \frac{s + \omega_b}{M_s(s + \omega_b\varepsilon)}$$

To define $W_u(s)$, we select the maximum gain M_u of $K(s)S(s)$, the controller bandwidth ω_{bc} and a small $\varepsilon_1 > 0$ such that:

$$W_u(s) = \frac{s + \omega_{bc}}{M_u(\varepsilon_1 s + \omega_{bc})} \, .$$

Figure 5 shows the frequency responses of $W_e^{-1}(s)$ and $W_u^{-1}(s)$. In the $\mathscr{H}_\infty$ design procedure, they are selected in order to guarantee

$$||S(s)||_\infty \leq ||W_e^{-1}(s)||_\infty \tag{11}$$

and

$$||K(s)S(s)||_\infty \leq ||W_u^{-1}(s)||_\infty. \tag{12}$$

Considering the above weighting functions and the state space representation of SEAs, Eq. 6, the state-space realization of the augmented plant $P(s)$ is given by the following matrices referring to Eq. 7:

$$A=\begin{bmatrix} 0 & I & 0 & 0 \\ -\frac{K_s}{m_m} & -\frac{b_m}{m_m} & 0 & 0 \\ 0 & 0 & A_{W_u} & 0 \\ B_{W_e} & 0 & 0 & A_{W_e} \end{bmatrix}, B_1=\begin{bmatrix} 0 & 0 \\ \frac{K_s}{m_m} & 0 \\ 0 & 0 \\ 0 & B_{W_e} \end{bmatrix}, B_2=\begin{bmatrix} 0 \\ \frac{K_s}{m_m} \\ B_{W_u} \\ 0 \end{bmatrix},$$

$$C_1=\begin{bmatrix} D_{W_e} & 0 & 0 & C_{W_e} \\ 0 & 0 & C_{W_u} & 0 \end{bmatrix}, \quad C_2=\begin{bmatrix} 1 & 0 & 0 & 0 \end{bmatrix},$$

$$D_{11}=\begin{bmatrix} 0 & D_{W_e} \\ 0 & 0 \end{bmatrix}, \quad D_{12}=\begin{bmatrix} 0 \\ D_{W_u} \end{bmatrix}, \quad D_{21}=\begin{bmatrix} 0 & 1 \end{bmatrix}, \quad D_{22}=\begin{bmatrix} 0 \end{bmatrix}$$

where $(A_{W_u}, B_{W_u}, C_{W_u}, D_{W_u})$ is the state-space realization of the weighting function $W_u(s)$, and $(A_{W_e}, B_{W_e}, C_{W_e}, D_{W_e})$ of $W_e(s)$.

4. $\mathscr{H}_\infty$ IMPEDANCE CONTROL

In this section, it is proposed a impedance control strategy for series elastic actuators which considers $\mathscr{H}_\infty$ performance. First, it is defined a transfer function, $Z(s)$, which represent the desired impedance for the system. For the SEA model described in Section 2.1the impedance transfer function is given by:

$$Z(s)=\frac{X_l(s)}{F_l(s)}=\frac{1}{B_v s+K_v} \tag{13}$$

where B_v and K_v are the desired damping and stiffness coefficients, respectively. Regarding the definition of $Z(s)$, Figure 6 shows the block diagram of the proposed control strategy for the impedance control, where . It is also considered here the weighting functions $W_e(s)$ e $W_u(s)$ as defined in Section 3.

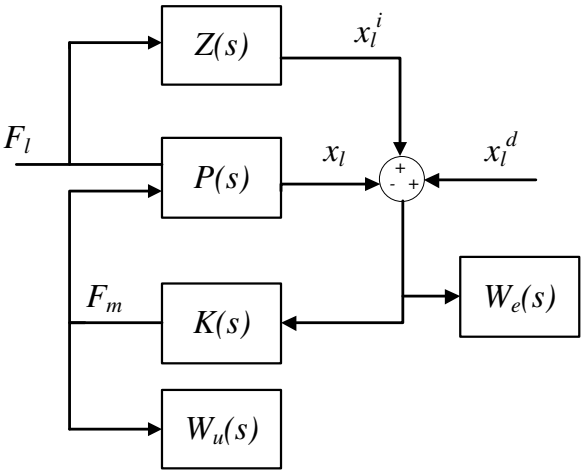

Figure 6. Diagrama controle impedancia com especificações no domínio da freqüência

With this control strategy, the robust controller $K(s)$ works by changing the end-effector position of an amount equal to the response of $Z(s)$ for the given input F_l, since the input of the controller are the current position plus the reference position imposed by the desired impedance. The controller design follows the procedure described in the previous section.

5. RESULTS

In this section it is presented simulated results obtained by applying the proposed robust $\mathscr{H}_\infty$ force control in the model of the SEA presented in Figure 3. The dynamic parameters of this model are given by: $m_m = 70Kg$, $K_s = 78.9KN/m$, $b_m = 13KN/m/s$.

The $\mathscr{H}_\infty$ force control was designed considering the weighting functions parameters shown in Table 1. Figure 7 shows the graphics of the sensitivity function $S(s)$ versus the weighting function $W_e^{-1}(s)$, and of $K(s)S(s)$ versus $W_u^{-1}(s)$ for the resulting controller. Note that the controlled plant curves are lower than the weighting functions for all frequency.

For comparison purposes, it was also designed a PID regarding the nominal model and the Ziegler-Nichols first method. The PID gains are given by $K_p = 21.6$, $K_v = 0.1$ and $K_i = 1000$.

Table 1. Weighting functions parameters.

M_s (dB)	ω_b (rad/s)	ε	M_u (dB)	ω_{bc} (rad/s)	ε_1
50	600	0.0015	50	10^5	0.01

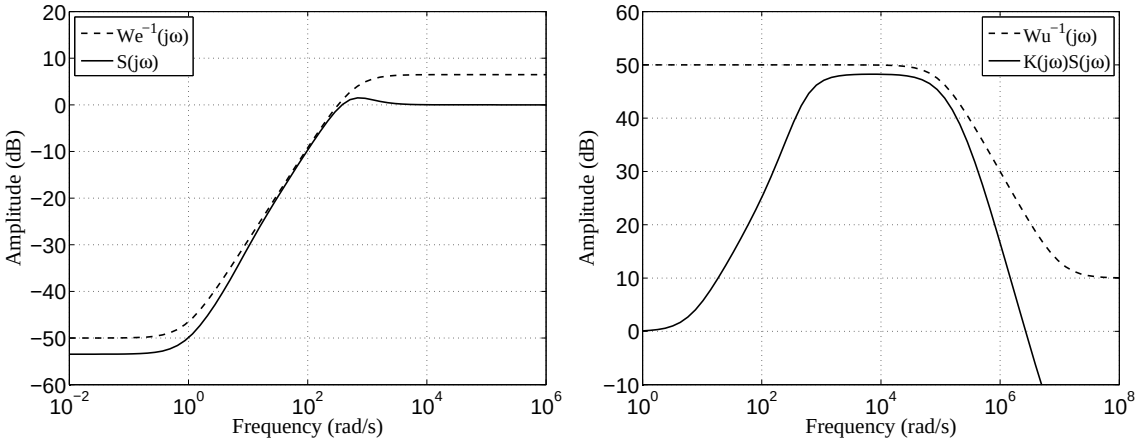

Figure 7. Sensitivity function $S(s)$ versus $W_e^{-1}(s)$ and $K(s)S(s)$ versus $W_u^{-1}(s)$.

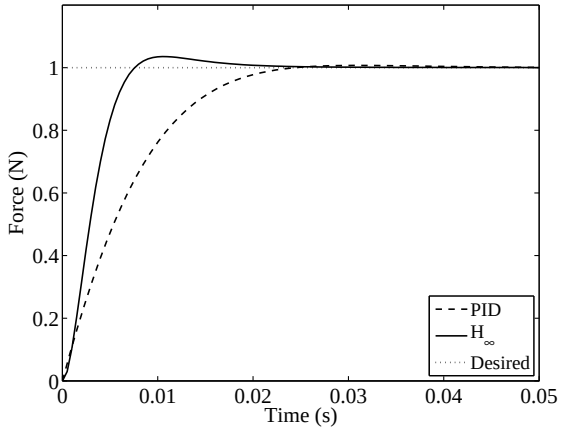

Figure 8. Closed loop step response considering the robust $\mathscr{H}_\infty$ controller and the PID controller.

To evaluate the proposed controllers we carried out two scenarios. First, parametric uncertainties of 50% are introduced in the dynamic parameters m_m, b_m and K_s. The step response of the closed loop system is obtained for both controllers. Figure 8 shows the curves, one can note that the robust controller presents a faster response, with small overshoot. On the other hand, the PID controller presents a overdamped response. Figure 9 shows the Bode graphic for the closed loop tranfer function for the proposed controller. The $\mathscr{H}_\infty$ force control increases the bandwidth of the system over the PID controller.

To test the controllers' disturbance rejection properties, in the second scenario it is add to the force computed by the controllers an exponentially attenuated sinusoidal external disturbance of the form:

$$w(t) = Ae^{\frac{-(t-t_f)^2}{2\sigma^2}} sin(\omega t),$$

where A is the maximum disturbance amplitude, t_f and σ are respectively the mean and standard deviation of the attenuation function, and ω is the frequency of the sinusoid. Fig. 10 presents the torque disturbances for $A = 50$ N, $\omega = 2$ rad/s, $t_f = 5$ s, and $\sigma_i = 1$. The high value of amplitude is to increase the disturbance effect on the output response.

Also, the force reference input is now defined as a trapezoidal signal, starting from zero and reaching $10N$ after 1 second, and maintaining this value for 3 seconds. Negative force reference is also taken into account. Figure 11 shows the closed loop response with the application of the external disturbance, for the trapezoidal force reference.

One can evaluate that the the robust $\mathscr{H}_\infty$ force control presents a better response, following the reference signal and rejecting the external disturbance properly. Although the PID controller follows perfectly the reference signal when the disturbance is small, its response degrates considerably with the increase of the disturbance.

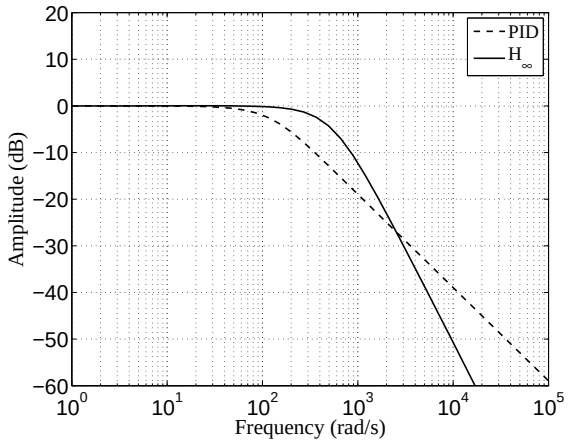

Figure 9. Closed loop frequency response for both robust $\mathscr{H}_\infty$ and the PID controllers.

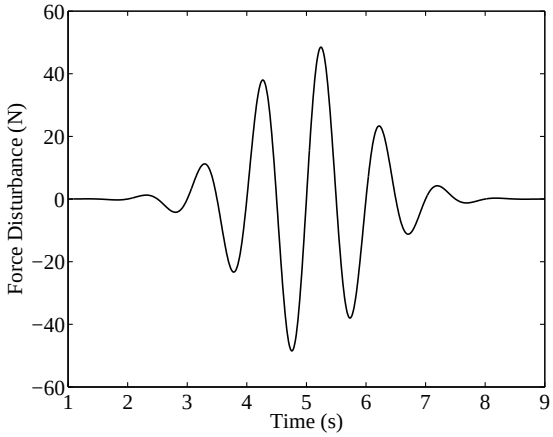

Figure 10. External disturbance applied to the plant for the trapezoidal force reference input.

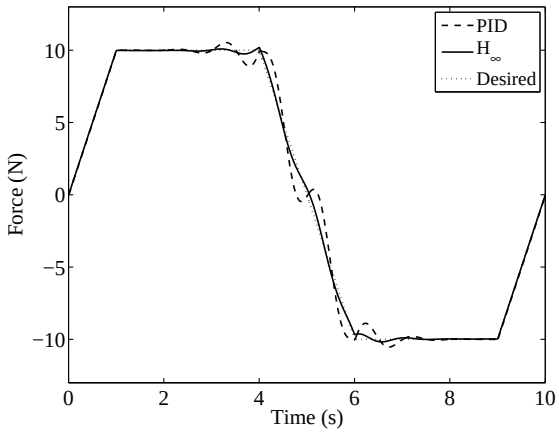

Figure 11. Closed loop response considering the robust $\mathscr{H}_\infty$ controller and the PID controller, the trapezoidal force reference and the external disturbance.

For the robust $\mathscr{H}_\infty$ impedance control, a trapezoidal position reference is defined and a disturbance with the same shape described before is introduced in the system input. The desired impedance transfer function is defined as in Eq. 13 with $B_v = 1$ Ns/mm and $K_v = 60$ N/mm. Figure 12 shows the results for the robust impedance control.

It is also simulated a zero reference trajectory for the end-effector. However, the external disturbances is maintained. The main purpose is to verify if the end-effector follows the desired trajectory generated by the impedance transfer function. Figure 13 shows the desired trajectory given by the impedance transfer function and the system response. Note that, since the desired impedance is basically defined as a spring-like behavior ($K_v >> B_v$), the desired trajectory is proportional to the disturbance force approximately by a factor of K_v.

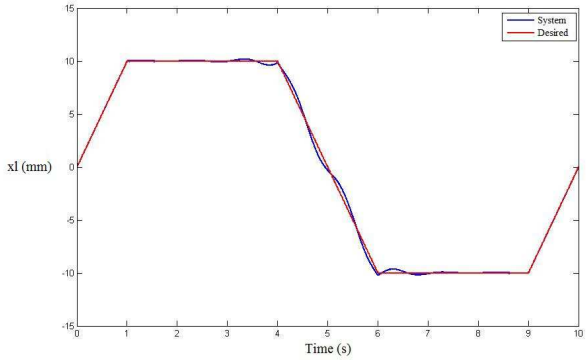

Figure 12. Closed loop response considering the $\mathscr{H}_\infty$ impedance control for a trapezoidal position reference.

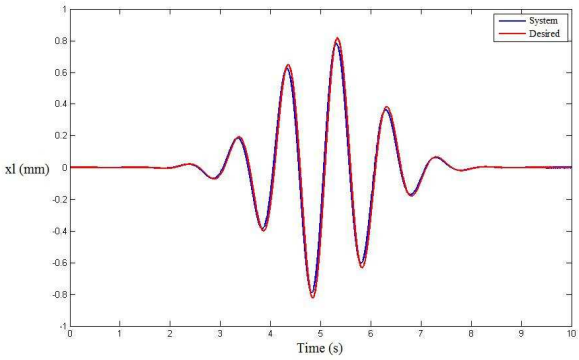

Figure 13. Closed loop response considering the $\mathscr{H}_\infty$ impedance control for a zero position reference and an external disturbance.

6. CONCLUSIONS

This paper presents the results of $\mathscr{H}_\infty$ force and impedance control for series elastic actuators. SEAs are devices where elastic components are introduced between the motor's output and the load. It is possible to measure the force applied to the load and to control it measuring the deflection of the elastic components. It is shown that the $\mathscr{H}_\infty$ force controller increased the bandwidth over the PID controller and rejects external disturbances properly. It is also shown a control strategy for impedance control, where the desired transfer function impedance is included in the augmented plant of the system. The results shows the end-effector position follows the external forces with the given desired impedance. The proposed controllers will be implemented in the actual SEAs attached to the exoskeleton for trajectory tracking based on the ZMP (Zero Moment Point) or CPG (Central Pattern Generator).

7. ACKNOWLEDGMENTS

This work was supported by São Paulo Research Foundation (FAPESP) under grant no. 2008/09530-4.

8. REFERENCES

Blaya, J.B. and Herr, H., 2004. "Adaptive control of a variable-impedance ankle-foot orthosis to assist drop-foot gait". *IEEE Transactions on Neural Systems and Rehabilitation Engineering*, Vol. 12, No. 1.

Chang, Y.C., 2000. "Neural network-based $\mathscr{H}_\infty$ tracking control for robotic systems". *IEE Proceedings of Control Theory Applications*, Vol. 147, No. 3, pp. 303–311.

Chen, B.S., Lee, T.S. and Feng, J.H., 1994. "A nonlinear $\mathscr{H}_\infty$ control design in robotic systems under parameter perturbation and external disturbance". *International Journal of Control*, Vol. 59, No. 2, pp. 439–461.

Chu, A., Kazerooni, H. and Zoss, A., 2005. "On the biomimetic design of the Berkeley Lower Extremity Exoskeleton (BLEEX)". In *Proceedings of the the 2005 IEEE International Conference on Robotics and Automation*. Barcelona, pp. 4345 – 4352.

Kazerooni, H., 2005. "Exoskeletons for human power augmentation". In *Proceedings of the 2005 IEEE/RSJ International Conference on Intelligent Robots and Systems*. Edmonton,Canada.

Kim, S., Anwar, G. and Kazerooni, H., 2004. "High-speed communication network for controls with the application on

the exoskeleton". In *Proceedings of the 2004 American Control Conference*. Boston, USA.

Paluska, D. and Herr, H., 2006. "The effect of series elasticity on actuator power and work output: Implications for robotic and prosthetic joint design". *Robotics and Autonomous Systems*, Vol. 54, pp. 667–673.

Pratt, G. and Williamson, M., 1995. "Series elastic actuators". In *Proceedings of the 1995 IEEE/RSJ International Conference on Intelligent Robots and Systems*. Pittsburgh, Vol. 1, pp. 399 – 406.

Pratt, J., Krupp, B.T. and Morse, C.J., 2004. "The roboknee: An exoskeleton for enhancing strenght and endurance during walking". In *Proceedings of the 2004 IEEE International Conference on Robotics and Automation*. New Orleans, LA.

Pratt, J. and Pratt, G., 1998. "Exploiting natural dynamics in the control of a planar bipedal walking robot". In *Proceedings of the Thirty-Sixth Annual Allerton Conference on Communication, Control, and Computing*. Urbana-Champaign, Illinois, pp. 561 – 568.

Robinson, D.W., Pratt, J., Paluska, D. and Pratt, G., 1999. "Series elastic actuator development for a biomimetic walking robot". In *Proceedings of the 1999 IEEE/ASME International Conference on Advanced Intelligent Mechatronics*. Atlanta, pp. 561 – 568.

Safonov, M.G., Limebeer, D.J.N. and Chiang, R.Y., 1989. "Simplifying the $\mathscr{H}_\infty$ theory via loop shifting, matrix pencil and descriptor concepts". *International Journal of Control*, Vol. 50, No. 6, pp. 2467–2488.

Sage, H.G., de Mathelin, M.F. and Ostertag, E., 1999. "Robust control of robot manipulators: a survey". *International Journal of Control*, Vol. 72, No. 16, pp. 1498–1522.

Sensinger, J.W. and Weir, R.F., 2006. "Improvements to series elastic actuators". *Mechatronic and Embedded Systems and Applications*, pp. 1–7.

Walsh, C.J., Paluska, D.J., Pasch, K., Grand, W., Valiente, A. and Herr, H., 2006. "Development of a lightweight, underactuated expskeleton for load-carrying augmentation". In *Proceedings of the 2006 IEEE International Conference on Robotics and Automation*. Orlanda, Florida, pp. 3485–3491.

Zhou, K., Doyle, J.C. and Glover, K., 1995. *Robust and Optimal Control*. Prentice Hall.

Zoss, A., Kazerooni, H. and Chu, A., 2005. "On the mechanical design of the Berkeley Lower Extremity Exoskeleton (BLEEX)". In *Proceedings of the 2005 IEEE/RSJ International Conference on Intelligent Robots and Systems*. Edmonton, Canada, pp. 3465 – 3472.

9. Responsibility notice

The author(s) is (are) the only responsible for the printed material included in this paper